EUROPEAN LABORATORY FOR PARTICLE PHYSICS (CERN)

CERN-EP/99-027
24th February 1999

Measurement of the W Mass in e^+e^- Collisions at 183 GeV

The ALEPH Collaboration

Abstract

The mass of the W boson is obtained from reconstructed invariant mass distributions in W-pair events. The sample of W pairs is selected from 57 pb^{-1} collected with the ALEPH detector in 1997 at a centre-of-mass energy of 183 GeV. The invariant mass distributions of reweighted Monte Carlo events are fitted separately to the experimental distributions in the $\mathrm{q\bar{q}q\bar{q}}$ and all $\ell\nu\mathrm{q\bar{q}}$ channels to give the following W masses:

$$\begin{aligned} m_{\mathrm{W}}^{hadronic} &= 80.461 \pm 0.177(\mathrm{stat.}) \pm 0.045(\mathrm{syst.}) \pm 0.056(\mathrm{theory})\ \mathrm{GeV}/c^2, \\ m_{\mathrm{W}}^{semileptonic} &= 80.326 \pm 0.184(\mathrm{stat.}) \pm 0.040(\mathrm{syst.})\ \mathrm{GeV}/c^2, \end{aligned}$$

where the theory error represents the possible effects of final state interactions. The combination of these two measurements, including the LEP energy calibration uncertainty, gives

$$m_{\mathrm{W}} = 80.393 \pm 0.128(\mathrm{stat.}) \pm 0.041(\mathrm{syst.}) \pm 0.028(\mathrm{theory}) \pm 0.021(\mathrm{LEP})\ \mathrm{GeV}/c^2.$$

(submitted to Phys. Lett. B)

The ALEPH Collaboration

R. Barate, D. Decamp, P. Ghez, C. Goy, S. Jezequel, J.-P. Lees, F. Martin, E. Merle, M.-N. Minard, B. Pietrzyk

Laboratoire de Physique des Particules (LAPP), IN^{2}P^3-CNRS, F-74019 Annecy-le-Vieux Cedex, France

R. Alemany, M.P. Casado, M. Chmeissani, J.M. Crespo, E. Fernandez, M. Fernandez-Bosman, Ll. Garrido,[15] E. Graugès, A. Juste, M. Martinez, G. Merino, R. Miquel, Ll.M. Mir, P. Morawitz, A. Pacheco, I.C. Park, I. Riu

Institut de Física d'Altes Energies, Universitat Autònoma de Barcelona, 08193 Bellaterra (Barcelona), E-Spain[7]

A. Colaleo, D. Creanza, M. de Palma, G. Gelao, G. Iaselli, G. Maggi, M. Maggi, S. Nuzzo, A. Ranieri, G. Raso, F. Ruggieri, G. Selvaggi, L. Silvestris, P. Tempesta, A. Tricomi,[3] G. Zito

Dipartimento di Fisica, INFN Sezione di Bari, I-70126 Bari, Italy

X. Huang, J. Lin, Q. Ouyang, T. Wang, Y. Xie, R. Xu, S. Xue, J. Zhang, L. Zhang, W. Zhao

Institute of High-Energy Physics, Academia Sinica, Beijing, The People's Republic of China[8]

D. Abbaneo, U. Becker,[19] G. Boix,[6] M. Cattaneo, V. Ciulli, G. Dissertori, H. Drevermann, R.W. Forty, M. Frank, F. Gianotti, A.W. Halley, J.B. Hansen, J. Harvey, P. Janot, B. Jost, I. Lehraus, O. Leroy, C. Loomis, P. Maley, P. Mato, A. Minten, A. Moutoussi, F. Ranjard, L. Rolandi, D. Rousseau, D. Schlatter, M. Schmitt,[20] O. Schneider,[23] W. Tejessy, F. Teubert, I.R. Tomalin, E. Tournefier, M. Vreeswijk, A.E. Wright

European Laboratory for Particle Physics (CERN), CH-1211 Geneva 23, Switzerland

Z. Ajaltouni, F. Badaud G. Chazelle, O. Deschamps, S. Dessagne, A. Falvard, C. Ferdi, P. Gay, C. Guicheney, P. Henrard, J. Jousset, B. Michel, S. Monteil, J-C. Montret, D. Pallin, P. Perret, F. Podlyski

Laboratoire de Physique Corpusculaire, Université Blaise Pascal, IN^{2}P^3-CNRS, Clermont-Ferrand, F-63177 Aubière, France

J.D. Hansen, J.R. Hansen, P.H. Hansen, B.S. Nilsson, B. Rensch, A. Wäänänen

Niels Bohr Institute, 2100 Copenhagen, DK-Denmark[9]

G. Daskalakis, A. Kyriakis, C. Markou, E. Simopoulou, A. Vayaki

Nuclear Research Center Demokritos (NRCD), GR-15310 Attiki, Greece

A. Blondel, J.-C. Brient, F. Machefert, A. Rougé, M. Swynghedauw, R. Tanaka, A. Valassi,[12] H. Videau

Laboratoire de Physique Nucléaire et des Hautes Energies, Ecole Polytechnique, IN^{2}P^3-CNRS, F-91128 Palaiseau Cedex, France

E. Focardi, G. Parrini, K. Zachariadou

Dipartimento di Fisica, Università di Firenze, INFN Sezione di Firenze, I-50125 Firenze, Italy

R. Cavanaugh, M. Corden, C. Georgiopoulos

Supercomputer Computations Research Institute, Florida State University, Tallahassee, FL 32306-4052, USA [13,14]

A. Antonelli, G. Bencivenni, G. Bologna,[4] F. Bossi, P. Campana, G. Capon, F. Cerutti, V. Chiarella, P. Laurelli, G. Mannocchi,[5] F. Murtas, G.P. Murtas, L. Passalacqua, M. Pepe-Altarelli[1]

Laboratori Nazionali dell'INFN (LNF-INFN), I-00044 Frascati, Italy

M. Chalmers, L. Curtis, J.G. Lynch, P. Negus, V. O'Shea, B. Raeven, C. Raine, D. Smith, P. Teixeira-Dias, A.S. Thompson, J.J. Ward

Department of Physics and Astronomy, University of Glasgow, Glasgow G12 8QQ,United Kingdom[10]

O. Buchmüller, S. Dhamotharan, C. Geweniger, P. Hanke, G. Hansper, V. Hepp, E.E. Kluge, A.L. Onk, A. Putzer, G. Schmidt, J. Sommer, K. Tittel, S. Werner,[19] M. Wunsch

Institut für Hochenergiephysik, Universität Heidelberg, D-69120 Heidelberg, Germany[16]

R. Beuselinck, D.M. Binnie, W. Cameron, P.J. Dornan,[1] M. Girone, S. Goodsir, N. Marinelli, E.B. Martin, J. Nash, J. Nowell, J.K. Sedgbeer, P. Spagnolo, E. Thomson, M.D. Williams

Department of Physics, Imperial College, London SW7 2BZ, United Kingdom[10]

V.M. Ghete, P. Girtler, E. Kneringer, D. Kuhn, G. Rudolph

Institut für Experimentalphysik, Universität Innsbruck, A-6020 Innsbruck, Austria[18]

A.P. Betteridge, C.K. Bowdery, P.G. Buck, P. Colrain, G. Crawford, G. Ellis, A.J. Finch, F. Foster, G. Hughes, R.W.L. Jones, N.A. Robertson, M.I. Williams

Department of Physics, University of Lancaster, Lancaster LA1 4YB, United Kingdom[10]

P. van Gemmeren, I. Giehl, F. Hölldorfer, C. Hoffmann, K. Jakobs, K. Kleinknecht, M. Kröcker, H.-A. Nürnberger, G. Quast, B. Renk, E. Rohne, H.-G. Sander, S. Schmeling, H. Wachsmuth C. Zeitnitz, T. Ziegler

Institut für Physik, Universität Mainz, D-55099 Mainz, Germany[16]

J.J. Aubert, C. Benchouk, A. Bonissent, J. Carr,[1] P. Coyle, A. Ealet, D. Fouchez, F. Motsch, P. Payre, M. Talby, M. Thulasidas, A. Tilquin

Centre de Physique des Particules, Faculté des Sciences de Luminy, IN^{2}P^3-CNRS, F-13288 Marseille, France

M. Aleppo, M. Antonelli, F. Ragusa

Dipartimento di Fisica, Università di Milano e INFN Sezione di Milano, I-20133 Milano, Italy.

R. Berlich, V. Büscher, H. Dietl, G. Ganis, K. Hüttmann, G. Lütjens, C. Mannert, W. Männer, H.-G. Moser, S. Schael, R. Settles, H. Seywerd, H. Stenzel, W. Wiedenmann, G. Wolf

Max-Planck-Institut für Physik, Werner-Heisenberg-Institut, D-80805 München, Germany[16]

P. Azzurri, J. Boucrot, O. Callot, S. Chen, M. Davier, L. Duflot, J.-F. Grivaz, Ph. Heusse, A. Jacholkowska, M. Kado, J. Lefrançois, L. Serin, J.-J. Veillet, I. Videau,[1] J.-B. de Vivie de Régie, D. Zerwas

Laboratoire de l'Accélérateur Linéaire, Université de Paris-Sud, IN^{2}P^3-CNRS, F-91898 Orsay Cedex, France

G. Bagliesi, S. Bettarini, T. Boccali, C. Bozzi,[24] G. Calderini, R. Dell'Orso, G. D'Onofrio, I. Ferrante, A. Giassi, A. Gregorio, F. Ligabue, A. Lusiani, P.S. Marrocchesi, A. Messineo, F. Palla, G. Rizzo, G. Sanguinetti, A. Sciabà, G. Sguazzoni, R. Tenchini, C. Vannini, A. Venturi, P.G. Verdini

Dipartimento di Fisica dell'Università, INFN Sezione di Pisa, e Scuola Normale Superiore, I-56010 Pisa, Italy

G.A. Blair, J. Coles, G. Cowan, M.G. Green, D.E. Hutchcroft, L.T. Jones, T. Medcalf, J.A. Strong, J.H. von Wimmersperg-Toeller

Department of Physics, Royal Holloway & Bedford New College, University of London, Surrey TW20 OEX, United Kingdom[10]

D.R. Botterill, R.W. Clifft, T.R. Edgecock, P.R. Norton, J.C. Thompson

Particle Physics Dept., Rutherford Appleton Laboratory, Chilton, Didcot, Oxon OX11 OQX, United Kingdom[10]

B. Bloch-Devaux, P. Colas, B. Fabbro, G. Faïf, E. Lançon, M.-C. Lemaire, E. Locci, P. Perez, H. Przysiezniak, J. Rander, J.-F. Renardy, A. Rosowsky, A. Trabelsi,[21] B. Tuchming, B. Vallage

CEA, DAPNIA/Service de Physique des Particules, CE-Saclay, F-91191 Gif-sur-Yvette Cedex, France[17]

S.N. Black, J.H. Dann, H.Y. Kim, N. Konstantinidis, A.M. Litke, M.A. McNeil, G. Taylor

Institute for Particle Physics, University of California at Santa Cruz, Santa Cruz, CA 95064, USA[22]

C.N. Booth, S. Cartwright, F. Combley, P.N. Hodgson, M.S. Kelly, M. Lehto, L.F. Thompson

Department of Physics, University of Sheffield, Sheffield S3 7RH, United Kingdom[10]

K. Affholderbach, A. Böhrer, S. Brandt, C. Grupen, A. Misiejuk, G. Prange, U. Sieler

Fachbereich Physik, Universität Siegen, D-57068 Siegen, Germany[16]

G. Giannini, B. Gobbo

Dipartimento di Fisica, Università di Trieste e INFN Sezione di Trieste, I-34127 Trieste, Italy

J. Putz, J. Rothberg, S. Wasserbaech, R.W. Williams

Experimental Elementary Particle Physics, University of Washington, WA 98195 Seattle, U.S.A.

S.R. Armstrong, E. Charles, P. Elmer, D.P.S. Ferguson, Y. Gao, S. González, T.C. Greening, O.J. Hayes, H. Hu, S. Jin, P.A. McNamara III, J.M. Nachtman,[2] J. Nielsen, W. Orejudos, Y.B. Pan, Y. Saadi, I.J. Scott, J. Walsh, Sau Lan Wu, X. Wu, G. Zobernig

Department of Physics, University of Wisconsin, Madison, WI 53706, USA[11]

[1]Also at CERN, 1211 Geneva 23, Switzerland.
[2]Now at University of California at Los Angeles (UCLA), Los Angeles, CA 90024, U.S.A.
[3]Also at Dipartimento di Fisica, INFN Sezione di Catania, 95129 Catania, Italy.
[4]Also Istituto di Fisica Generale, Università di Torino, 10125 Torino, Italy.
[5]Also Istituto di Cosmo-Geofisica del C.N.R., Torino, Italy.
[6]Supported by the Commission of the European Communities, contract ERBFMBICT982894.
[7]Supported by CICYT, Spain.
[8]Supported by the National Science Foundation of China.
[9]Supported by the Danish Natural Science Research Council.
[10]Supported by the UK Particle Physics and Astronomy Research Council.
[11]Supported by the US Department of Energy, grant DE-FG0295-ER40896.
[12]Now at LAL, 91898 Orsay, France.
[13]Supported by the US Department of Energy, contract DE-FG05-92ER40742.
[14]Supported by the US Department of Energy, contract DE-FC05-85ER250000.
[15]Permanent address: Universitat de Barcelona, 08208 Barcelona, Spain.
[16]Supported by the Bundesministerium für Bildung, Wissenschaft, Forschung und Technologie, Germany.
[17]Supported by the Direction des Sciences de la Matière, C.E.A.
[18]Supported by Fonds zur Förderung der wissenschaftlichen Forschung, Austria.
[19]Now at SAP AG, 69185 Walldorf, Germany
[20]Now at Harvard University, Cambridge, MA 02138, U.S.A.
[21]Now at Département de Physique, Faculté des Sciences de Tunis, 1060 Le Belvédère, Tunisia.
[22]Supported by the US Department of Energy, grant DE-FG03-92ER40689.
[23]Now at Université de Lausanne, 1015 Lausanne, Switzerland.
[24]Now at INFN Sezione di Ferrara, 44100 Ferrara, Italy.

1 Introduction

Pairs of W bosons have been produced at LEP since June 1996, when the centre-of-mass energy of the colliding beams reached the W-pair threshold near 161 GeV. At this energy, first measurements of the W mass at LEP were made using the measured cross sections [1, 2]. A larger sample of W pairs was collected from 10.65 pb^{-1} at 172 GeV in 1996, allowing the W mass to be measured from the direct reconstruction of the invariant mass of its decay products for the first time [3, 4]. Measurements have also been made at the Tevatron $\mathrm{p\bar{p}}$ Collider using large samples of single W's decaying into leptons [5].

This paper describes the ALEPH measurement of the W mass by direct reconstruction in both the $\mathrm{WW} \to \mathrm{q\bar{q}q\bar{q}}$ (denoted 4q) and $\mathrm{WW} \to \ell\nu\mathrm{q\bar{q}}$ channels from a much larger sample of data collected in 1997. The integrated luminosities were 0.17 pb^{-1}, 3.92 pb^{-1}, 50.79 pb^{-1}, and 1.93 pb^{-1} at centre-of-mass (CM) energies of 180.83, 181.72, 182.69 and 183.81 GeV, respectively. The luminosity weighted CM energy is 182.655 GeV. A high statistics run at 91.2 GeV of 2.5 pb^{-1} provided a large sample of Z decays for calibration. The paper is organised as follows. In sections 2 and 3, the important properties of the ALEPH detector for this analysis are recalled and a brief description is given of the Monte Carlo event generators for the processes involved. Sections 4, 5 and 6 describe the event selection and mass reconstruction procedures in the different channels. Compared with the earlier analysis of the much smaller data sample at 172 GeV [3], a new kinematic fitting method has been adopted for all $\mathrm{WW} \to \ell\nu\mathrm{q\bar{q}}$ channels and a two-dimensional Monte Carlo reweighting procedure introduced in the 4q channel. Sections 7 and 8 describe the stability checks made of the measurement and all studies of systematic errors. Finally, the measurements of the W mass in each channel are combined and then added to previously published results at 172 and 161 GeV, taking into account common sources of systematic errors.

2 The ALEPH detector

A detailed description of the ALEPH detector can be found in Ref. [6] and of its performance in Ref. [7]. Charged particles are detected in the central part of the detector. From the beam crossing point outwards, a silicon vertex detector, a cylindrical drift chamber and a large time projection chamber (TPC) measure up to 31 coordinates along the charged particle trajectories. A 1.5 T axial magnetic field, provided by a superconducting solenoidal coil, yields a resolution of $\delta p_T/p_T = 6 \times 10^{-4} p_T \oplus 0.005$ (p_T in GeV/c). Charged particle tracks reconstructed with at least four hits in the TPC and originating from within a cylinder of 2 cm radius and 20 cm length, centred on the nominal interaction point and parallel to the beam axis, are called *good tracks*.

Electrons and photons are identified in the electromagnetic calorimeter (ECAL) by their characteristic longitudinal and transverse shower development. The calorimeter, a lead/wire-plane sampling device with fine readout segmentation and total thickness of 22 radiation lengths at normal incidence, provides a relative energy resolution of $0.180/\sqrt{E} + 0.009$ (E in GeV).

Muons are identified by their penetration pattern in the hadron calorimeter (HCAL), a 1.2 m thick iron yoke instrumented with 23 layers of streamer tubes, together with two surrounding layers of muon chambers. In association with the electromagnetic calorimeter,

the hadron calorimeter also provides a measurement of the energy of charged and neutral hadrons with a relative resolution of $0.85/\sqrt{E}$ (E in GeV).

The total visible energy and momentum, and thus the missing energy, are evaluated by an energy flow reconstruction algorithm [7] which combines all of the above measurements, supplemented at low polar angles by the energy detected in the luminosity calorimeters. The algorithm also provides a list of charged and neutral reconstructed particles, called *energy flow objects*, from which jets are reconstructed with a typical angular resolution of 30 mrad in space. The jet energy resolution is approximately $\sigma_E = (0.6\sqrt{E} + 0.6)\text{GeV} \times (1 + \cos^2\theta)$, where E (in GeV) and θ are the jet energy and polar angle relative to the z axis along the e^- beam direction.

A high statistics study of the $Z \to q\bar{q}$ events collected at 91.2 GeV enables the simulation of jets with energies which lie in the mid range of those reconstructed from W hadronic decays to be re-calibrated. These studies show that 46 GeV jets are well simulated at all values of θ with the largest discrepancy ($\sim$1.5%) being in the overlap region between barrel and endcaps. The Monte Carlo reconstructed jet energies are corrected using a parametrisation of this discrepancy as a function of θ.

3 Monte Carlo samples

The W mass is extracted by comparing the experimental invariant mass distributions to the corresponding Monte Carlo distributions, where generated events are processed through a full simulation of the ALEPH detector response and through the same reconstruction chain. The `KORALW` event generator, version 1.21 [8], is used to produce the reference W pair events. Within `KORALW` all four-fermion (4-f) diagrams producing WW - like final states are computed with the `GRACE` package [9] with constant W and Z widths in the propagators. The `JETSET` [10] package with parameters tuned at the Z takes care of hadronisation. Final state interactions are not included. A reference sample of 400k events to all decay modes, equivalent to an integrated luminosity of 24.97 fb^{-1}, was generated at a CM energy of 183 GeV with a W mass of 80.35 GeV/c^2. The decay width was taken from Standard Model predictions to be 2.094 GeV/c^2 at this mass. From this reference sample, 20k 4q events were used exclusively for the training of a neural network leaving the remainder for the reweighting analysis in this channel. All 400k events were used as a reference sample in the analysis of the $\ell\nu q\bar{q}$ channels. Four additional samples of 50k events each were generated with W masses of 79.85, 80.10, 80.60, 80.85 GeV/c^2 for checking the stability of the results. In addition, an independent sample of 300k W pair events was generated with `KORALW` restricted to the doubly resonant CC03 diagrams [11]. This sample is used to determine the selection efficiencies and parametrise the corrections used in the kinematic fitting.

All background reactions were fully simulated at 183 GeV. `PYTHIA` [10] was used to generate 500k $e^+e^- \to q\bar{q}(\gamma)$ events corresponding to an integrated luminosity of 4.65 fb^{-1}. Also 20k ZZ and 60k Zee events were generated with `PYTHIA`, the latter with a minimum $Z(\gamma^*)$ invariant mass of 2 GeV/c^2. Events with a flavour content that could originate from WW production are explicitly rejected from the ZZ sample to avoid double counting with the `KORALW` 4-f sample. The $e^+e^- \to We\nu$ process was simulated by `PYTHIA` with the electrons generated over the phase space allowed in the production of the semileptonic 4-f events. Two-photon ($\gamma\gamma$) reactions into leptons and hadrons were simulated with

the PHOT02 [12] and PYTHIA generators but no events survived the selection cuts for any channel. KORALZ [13] and UNIBAB [14] were used for dilepton final states.

4 Event selections

In the following subsections, the event selections are described for the four types of events considered: $W^+W^- \to q\bar{q}q\bar{q}$, $W^+W^- \to e\nu q\bar{q}$, $W^+W^- \to \mu\nu q\bar{q}$ and $WW \to \tau\nu q\bar{q}$. Purely leptonic events are not considered in this paper. The selection efficiencies for each channel are calculated using the CC03 Monte Carlo sample. They are summarised in Table 1 together with the expected observable cross sections from all contributing processes. The number of signal events expected from the CC03 sample is within ∼1% of the 4-f Monte Carlo prediction for each channel.

4.1 $W^+W^- \to q\bar{q}q\bar{q}$ events

At 183 GeV the main source of background in the 4q channel is $e^+e^- \to q\bar{q}(\gamma)$ production, followed by the $e^+e^- \to WW \to \ell\nu q\bar{q}$ and $e^+e^- \to ZZ$ processes. To select hadronic decays, the following preselection cuts are applied: the event longitudinal momentum (p_L) relative to the beam axis must satisfy $|p_L| \leq 0.95(M_{vis} - M_Z)$, where M_{vis} is the reconstructed invariant mass of all observed energy flow objects, and the event sphericity must be greater than 0.03. The remaining events are forced into four jets using the DURHAM-P algorithm where the objects are clustered by their three-momenta and then each jet four-momentum is recalculated taking the object masses into account (the DURHAM-PE scheme). This procedure combines efficient clustering with minimal bias in the reconstruction of the candidate di-jet invariant masses. Further preselection cuts are applied to these jets: namely, the fraction of electromagnetic to total energy in a jet must be less than 0.95 and y_{34} (the value of the jet resolution parameter where a four-jet becomes a three-jet event) must be greater than 0.001.

An updated neural network [3] trained at 183 GeV is used to tag the preselected events, assigning an output ranging from −1 to +1. There are 19 input variables based on global event properties, heavy quark flavour tagging, jet properties and WW kinematics [15]. None of these variables depends directly on di-jet invariant masses. The jet related input variables are determined from kinematically fitted jet momenta (see section 5.1.1) leading to an improvement in the discriminating power of the network. The signal and $q\bar{q}(\gamma)$ events are well separated by the neural net output [15]. Keeping events with an output ≥ -0.3 leaves 461 accepted events in the data compared with 441.1 predicted events (362.1 from signal and 79.0 background). One event was also selected as a $WW \to \tau\nu q\bar{q}$ candidate. This event is kept by both selections to be consistent with the Monte Carlo where vetoing of alternative selections is not applied.

4.2 $W^+W^- \to e\nu q\bar{q}$ and $W^+W^- \to \mu\nu q\bar{q}$ events

The selection is based on the previous analysis at 172 GeV [3]. The charged track with the highest momentum component antiparallel to the missing momentum is chosen as the lepton candidate. Loose electron and muon identification criteria are then applied. In the selection of $e\nu q\bar{q}$ events, associated bremsstrahlung photons arising from interactions in

the detector material are identified and the photon energy added to that of the electron. These photons can appear either as an excess of energy in the ECAL electron cluster or as a separate deposit within 2.5° of the electron track impact point on ECAL. This correction is not applied when the electron is accompanied by other charged particles with summed momenta greater than 5 GeV/c within 6° of the candidate track. In addition, for all events a search is made for isolated final state (FSR) photons associated with the lepton. Such a photon must have an energy above 0.5 GeV, be closer to the candidate charged lepton track than to any other object or the beam axis and at least 40° away from any other good charged track. Their four-momenta are then combined. Any remaining energy deposits in ECAL within 1.5° of the extrapolated lepton candidate track or in HCAL within 2° are removed. The energy of the lepton candidate must exceed 21 GeV. The `DURHAM-PE` clustering algorithm is applied to all energy flow objects that are not used to construct the lepton four-momentum, and these are forced into two jets.

Then, the probability for an event to come from the signal process is constructed from the energy and isolation of the lepton as well as the total missing transverse momentum [1]. Cutting on this probability leaves 130 and 105 events in the electron and muon channels respectively. Monte Carlo studies predict 122.3 (109.5 signal, 12.8 background) and 118.8 (112.6 signal, 6.2 background) events, respectively, in good agreement.

4.3 $\mathrm{WW} \to \tau\nu\mathrm{q\bar{q}}$ events

The event selection procedure is based closely on methods developed earlier for the extraction of the cross section in this channel at 161 and 172 GeV. In summary, an event is selected if it passes a series of preselection cuts [1] and if it satisfies either a topological or a global selection [16]. Unlike the cross section analysis, a τ jet is always searched for as it is required for the measurement of the W mass. The event is vetoed if it is selected by either the e or μ selections, so that the semileptonic samples are independent. The number of events selected is 87, which is within 1.5σ of the Monte Carlo prediction of 101.9 (91.4 signal and 10.5 background).

5 Invariant mass reconstruction

5.1 $\mathrm{W^+W^-} \to \mathrm{q\bar{q}q\bar{q}}$ events

5.1.1 Kinematic fitting

Following a procedure developed previously to improve the mass resolution [3], a four-Constraint (4-C) kinematic fit employing Lagrange multipliers is performed on each event, the constraints imposed being the conservation of the combined three-momentum of the 4 jets and their total energy as provided by LEP. The fit assumes that the velocities (p/E) of the jets remain constant. Corrections are applied to the measured jet momenta and directions to take into account the effect of particle losses in the detector. The expectation values of these corrections and their resolutions are determined using the independent CC03 Monte Carlo sample by comparing the fully simulated jets in the detector with those built from the generated particles directly. The deviations are parametrised by Gaussians in bins of jet energy and θ. In this case, no account is taken of the effect of particle mis-associations in the clustering process at the generator level. For all events

Table 1: Expected observable cross sections for various processes after selection cuts for all channels. The quoted signal efficiencies and cross sections are determined using CC03 events with $m_{\mathrm{W}} = 80.35$ GeV/c^2. For the 4q channel, all events containing W decays are treated as signal. In the e and μ channels, only events of the appropriate type are considered as signal; whereas for the τ channel, e and μ events which pass the cuts and fail their own respective selections are included as signal. The two-photon background is negligible.

	σ_{cuts} (pb)			
Process	4q sel.	e sel.	μ sel.	τ sel.
$\mathrm{WW} \to \mathrm{q\bar{q}q\bar{q}}$	6.310	0.001	0.001	0.011
$\mathrm{WW} \to \mathrm{e}\nu\mathrm{q\bar{q}}$	0.008	1.927	0.001	0.165
$\mathrm{WW} \to \mu\nu\mathrm{q\bar{q}}$	0.021	0.003	1.981	0.138
$\mathrm{WW} \to \tau\nu\mathrm{q\bar{q}}$	0.036	0.072	0.073	1.294
$\mathrm{WW} \to \ell\nu\ell\nu$	0.000	0.003	0.002	0.000
$\mathrm{q\bar{q}}(\gamma)$	1.203	0.057	0.012	0.091
ZZ	0.188	0.011	0.014	0.034
Weν	0.000	0.009	0.001	0.054
Zee	0.006	0.060	0.002	0.006
$\tau\tau$	0.000	0.010	0.004	0.000
Efficiency (%)	88.9	82.3	84.9	69.4
Purity (%)	82.1	89.5	94.8	89.7

the kinematic fit converges successfully, producing a flat χ^2 probability distribution above 5% which is well described by the Monte Carlo.

The four fitted jets are combined into two di-jets in three different ways. For each of these combinations, two rescaled masses are determined [3]. The rescaled mass is given by $m_{ij}^{\mathrm{resc}}/m_{ij} = E_b/(E_i + E_j)$, where E_b is the beam energy and E_i, E_j are the jet energies.

5.1.2 Jet pairing

The jet pairing algorithm selects the combination with the smallest difference between the two rescaled masses unless this combination has the smallest sum of the two di-jet opening angles. In this case, the combination with the second smallest mass difference is selected. The combination with the third smallest mass difference is never reconsidered. Both masses for the selected combination must lie within the mass window 60 to 86 GeV/c^2 and at least one of the two masses must be between 74 and 86 GeV/c^2. If this condition fails then the other combination is accepted instead, provided its two masses satisfy the window criteria; otherwise the event is rejected. Monte Carlo studies show that this algorithm satisfies the criteria of minimal systematic bias on the final W mass whilst being efficient in finding the correct assignment of di-jet pairs. The fraction of kinematically fitted signal events surviving these criteria is 87%. Of these events, 90% are found to be the combination of di-jets which most closely match the directions of the original W di-quarks. The order of the two masses in the selected combination is then randomised to avoid correlations arising from energy ordering effects in the analysis. The final number of events accepted by the pairing algorithm is 384 compared with 367.5 predicted events (312.9 signal and 54.6 background events). Table 2 shows the predicted

fraction of signal events passing all analysis cuts and the final purities achieved in the event sample used for the mass extraction.

5.2 $\mathrm{WW} \to \ell\nu\mathrm{q}\bar{\mathrm{q}}$ events

A kinematic fitting package has been developed for the semileptonic channel which minimises a χ^2 of the form

$$S = \left(\frac{\Delta - <\Delta>}{\sigma_\Delta}\right)^T V^{-1} \left(\frac{\Delta - <\Delta>}{\sigma_\Delta}\right).$$

The vector Δ has 11 elements, corresponding to the 11 measured observables of a semileptonic event: 4 for each jet and 3 for the charged lepton since the mass is known. Each element describes the deviations due to detector resolution and acceptance of the measured from the true values of the observable. They are chosen to be normally distributed and minimally correlated. For each jet, the 4 vectors are:

$$\begin{aligned} \Delta_1 &= \triangle\beta \\ \Delta_2 &= \triangle E \\ \Delta_3 &= p_T^{(\triangle\theta)} \\ \Delta_4 &= p_T^{(\triangle\phi)} \end{aligned}$$

where $\triangle\beta$, $\triangle E$ are the differences between the measured and fitted jet velocities and energies respectively; $p_T^{(\triangle\theta)}$ and $p_T^{(\triangle\phi)}$ are the two orthogonal components of the transverse momentum of the measured relative to the fitted jet within and perpendicular to the plane containing the fitted jet and the z axis. In the τ channel and for events in the e and μ channels where calorimetric energy is added to the leptons, the same observables are used as for the jets, except $\triangle\beta$ is set equal to 0. Otherwise, the e or μ are described by the difference between the measured and fitted inverse radius of curvature $\triangle 1/r$, dip angle $\triangle tan\lambda$ and azimuthal direction at the event vertex $\triangle\phi^0$. The expected biases $<\Delta>$ and the resolutions σ_Δ, parametrised as a function of true energy and θ for the jets and leptons, as well as the average correlation matrix V are determined for each channel from the CC03 Monte Carlo.

A 2-C fit is applied where the hadronic and leptonic masses are made equal. Rather than imposing these constraints via Lagrange multiplier techniques, the 11 observables are transformed into 9 independent parameters which satisfy the conservation of energy and equality of the masses whilst covering the entire kinematically allowed phase space. The fit proceeds by varying these parameters, converting them to jet and lepton four-momenta which satisfy the constraints, computing the expected biases and resolutions defined above and minimising the χ^2. The 9 parameters are the 3 components of the lepton momentum, the W mass, the azimuthal angle of the W momentum with respect to the lepton momentum, the 2 jet masses and the polar and azimuthal decay angles of the hadronic W in its rest frame. Proper convergence of the fit is required, yielding a positive-definite error matrix.

For all channels, the fitted mass must lie in the window 74 to 91.5 GeV/c^2. In the case of the e and μ channels, events with a χ^2 probability less than 2% are also excluded. This improves the sample purity as shown in Fig. 1. For each channel respectively, 32 and 24 events either fail to converge in the fit or pass the χ^2 probability cut and a further 4 and

3 events lie outside the mass window. For the τ channel, no χ^2 probability cut is applied but 18 events fail to converge successfully and a further 12 events lie outside the mass window. The final number of events remaining from each channel for the measurement of the W mass and the corresponding predictions from the Monte Carlo after the final mass window cut are given in Table 2. They are consistent with the data and indicate that some events with large χ^2 are accompanied by ISR emission exceeding 0.5 GeV.

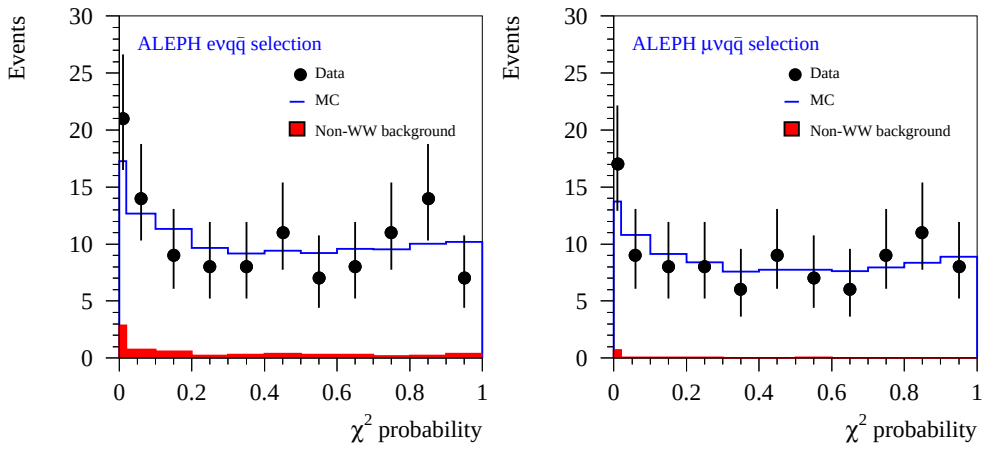

Figure 1: The χ^2 probability distribution for 2C kinematic fits in the e and μ channels.

Table 2: Final numbers of events (signal + background) remaining after all analysis cuts for the determination of the W mass in each channel. The corresponding CC03 Monte Carlo predictions (normalised to an integrated luminosity of 56.81 pb^{-1}) are tabulated together with the expected purities and fraction of signal events passing all cuts in each channel. Semileptonic Monte Carlo events which have failed their own channel selection but pass in another are included there as signal.

Process	4q	e	μ	τ
Predicted events	367.5	88.5	91.1	73.0
Observed events	384	94	78	57
Accepted (%)	76.9	64.6	67.9	51.0
Purity (%)	85.1	97.1	99.7	91.9

6 Extraction of the W mass

The W boson mass m_{W} is determined from the hadronic and semileptonic channels separately and a weighted average found, taking into account correlations in the systematic errors. For each channel, a binned Maximum Likelihood Monte Carlo reweighting

procedure developed previously [3] is employed to find the value of m_{W} which best fits the observed invariant mass distribution including background. Selected Monte Carlo signal events from the large 4-f reference sample are reweighted using CC03 matrix elements according to the single parameter to be fitted, m_{W}. The W width is set to 2.094 GeV/c^2 at 80.35 GeV/c^2 and varies with m_{W} according to the Standard Model.

At LEP1, the Z mass was defined using a running-width scheme in the Breit-Wigner propagator. However, a fixed-width scheme has been employed in generating all WW events with `KORALW`. As a result, to make both mass measurements consistent with each other, a positive shift of 27 MeV/c^2 is applied to the extracted W mass [17]. The sign and magnitude of the shift was verified by fitting appropriate fixed and running width Breit-Wigner functions to a large sample of generated events.

The statistical error on m_{W} is computed from the fits to the data distributions. Also, a large number of Monte Carlo subsamples are studied, each with the same number of events as the data, to evaluate the expected error from the RMS spread of fitted masses and the distribution of fit errors obtained.

6.1 The $\mathrm{q\bar{q}q\bar{q}}$ channel

The statistics at 183 GeV allow a true two-dimensional reweighting to be performed with the two rescaled masses per event (denoted the 2-D method). The event-by-event correlations in the data are then properly accounted for and lead to an improvement in statistical precision compared with the 1-D method [3] of approximately 10%. Using a binned two-dimensional probability density function, a maximum likelihood fit is performed to the data within the mass windows of 60 to 86 GeV/c^2 defined by the pairing algorithm (section 5.1). The bin sizes for the Monte Carlo events are chosen both for signal and summed backgrounds so that the number of events per bin for each case is approximately constant. A stable mass value and statistical error are obtained when the minimum number of Monte Carlo signal events in any bin is 60. The small residual background (0.5%) of semileptonic events is also reweighted.

6.2 The $\ell\nu\mathrm{q\bar{q}}$ channels

For each channel, the same procedure is employed as in ref. [3], namely a binned 1-D Monte Carlo reweighting to the distribution of the 2-C fitted masses within the region 74 to 91.5 GeV/c^2. For the e and μ channels, fixed bins of 0.5 GeV/c^2 are used whereas for the τ channel the bin intervals are varied depending on the density of Monte Carlo events.

7 Consistency and stability checks

7.1 Reproducibility of the reweighting procedure

The accuracy of the reweighting procedure is tested by comparing the fitted mass obtained from each of the five independent Monte Carlo samples generated with input masses between 79.85 and 80.85 GeV/c^2. The relationship between the fitted and true masses is found to be linear for all channels over this range and no significant offsets are observed.

For simplicity, CC03 matrix elements are used in the reweighting procedure instead of 4-f matrix elements. Replacing them with 4-f matrix elements from EXCALIBUR [18] in the e, μ and τ channels produces insignificant shifts of $\leq$10 MeV/c^2 in the fitted masses. The absence of any significant non-linearity in the relationship between fitted and true masses for all channels shows that CC03 matrix elements are sufficient for all channels at present.

7.2 Event selection and mass window dependence

The 4q events are selected from the data and Monte Carlo by requiring the neural network output to be larger than -0.3. This cut is varied in steps over the range -0.8 to $+0.8$ to investigate the stability of the fitted mass and error. Variations of up to 30 MeV/c^2 in the mass value are observed which are consistent with statistical fluctuations in the sample content. Similar studies are made with the semileptonic events by varying the probability cut and no significant shifts are found. In addition, the efficiencies and purities quoted in Table 2 do not depend on m_{W} over the range 79.85 to 80.85 GeV/c^2. A comparison of the shape of the data and corresponding Monte Carlo distributions is made for all variables used in the selection of events and in choosing the best combination of di-jets in the 4q channel. The stability of the result as a function of the mass windows used for both the data and reference Monte Carlo samples in the fits is checked for all decay channels. No significant discrepancies are observed.

8 Systematic uncertainties

The following subsections describe all the systematic errors considered for each decay channel. They are listed in Table 3 in two parts: (a) where there is some correlation between the channels and (b) where the errors are independent.

8.1 Fragmentation of the $\mathrm{W} \to \mathrm{q\bar{q}}$ decays

The JETSET fragmentation parameters, $\sigma_q, b, \Lambda_{QCD}$ and M_{min}, used in the generation of the reference WW sample are varied by up to $\pm 4\sigma$'s from their tuned values found at the Z. The effect on the fitted mass is less than 10 MeV/c^2 for all the channels. Similarly, there is no change in the mass when baryon production is disabled. However, a more significant effect is found when JETSET is replaced by HERWIG [19] to hadronise the partons in each event of the primary reference sample. In this way, two new reference samples are created using again JETSET in one case and HERWIG in the other where the fragmentation parameters are optimised at the Z using all hadronic events without flavour selection [20]. Fitted masses derived from Monte Carlo subsamples of the same size as the data by reweighting with the new reference samples in turn are compared and the average shift is quoted as the systematic error.

8.2 Calorimeter calibrations

The uncertainties in the global calibrations of the ECAL and HCAL energy were assessed to be $\pm 0.9\%$ and $\pm 2\%$ respectively. For the semileptonic channels, the effect of these

uncertainties is determined using 50 Monte Carlo samples of the same size as the data. The energy depositions in each event are scaled both up and down by these amounts, independently for the two calorimeters. The maximum mean shifts seen in m_{W} from the two directions are determined for each calorimeter and combined in quadrature to form the error. In the hadronic channel, the shifts are applied directly to the data rather than the Monte Carlo. In this case, common data samples are maintained to suppress statistical fluctuations.

8.3 Charged particle tracking

After the alignment of the data, small distortions remain in tracks, particularly in the forward regions of the detector. Corrections for these distortions, which are proportional to momentum and opposite in sign for positively and negatively charged particles, are determined by equalising the momenta of the two charged tracks in $\mathrm{Z} \to \mu^+\mu^-$ events. These corrections are applied to all tracks in the data sample. A conservative systematic error is evaluated for the semileptonic channels, which are more affected by these distortions, by applying the corrections to 50 Monte Carlo samples of the same size as the data and measuring the average change in m_{W}.

8.4 Jet corrections before the kinematic fit

The discrepancies found in matching reconstructed Monte Carlo jets to data are parametrised as a function of the jet polar angle θ to the beam axis (see section 5). To estimate the systematic error, two modified parametrisations are evaluated which accommodate the $\pm 1\sigma$ errors in these discrepancies taking into account the correlations. The largest shift observed in m_{W} for each channel when these modified parametrisations are used to correct the jet energies is taken as the systematic error.

8.5 Initial state radiation

`KORALW` [8] features QED initial state radiation up to $\mathcal{O}(\alpha^2 L^2)$, i.e., up to second order in the leading-log approximation. The effect of the missing higher order terms on the W mass measurement is estimated by weighting each event in a specially generated `KORALW` sample according to the calculated ratio of first to second order squared matrix elements: $\mathcal{O}(\alpha^1 L^1)/\mathcal{O}(\alpha^2 L^2)$. Treated as data, the weighted events selected in each channel are fitted to evaluate the mass and are compared with the corresponding unweighted events to provide an upper limit on the systematic shift.

8.6 Background contamination

For the 4q events, the expected background remaining after all analysis cuts is 15%. The relatively small size of the data sample does not permit a detailed comparison with Monte Carlo and so the technique using Z peak data [3] to evaluate the effect of any discrepancies in the background shape and normalisation is applied again, in this case to the 2-D mass distribution. The systematic uncertainty is smaller than at 172 GeV because the background shape is almost flat within the mass window.

For the semileptonic events, the error from this source is expected to be small because the total background is only a small fraction of the signal. The error due to the background shape is estimated using Z data, in the same way as for the hadronic channel. The uncertainty in the background normalisation is estimated by taking the largest discrepancy found in the ratio of data to Monte Carlo events in the e and μ channels where the probability is less than 0.1 and applying equally to all channels. The resulting error from both sources is very small in all channels.

8.7 Colour reconnection in the $q\bar{q}q\bar{q}$ channel

The colour reconnection effect is studied using Monte Carlo models based on variants of the parton evolution schemes in `JETSET`, `ARIADNE` [21] and `HERWIG`. In all cases, the input parameters for the variant considered are re-optimised to fit Z data.

For the `JETSET` study, a single sample of WW $\rightarrow q\bar{q}q\bar{q}$ events was generated (for practical reasons using `EXCALIBUR` [18]) and then hadronised in different ways to create (a) a fully simulated sample with no colour reconnection and (b) three other samples, labelled types I, II and II$'$ [22]. In type I, *all* events are reconnected with a probability which depends on the space-time overlap of the colour strings which have a significant transverse extension. The authors state that reconnecting all events is unrealistic and suggest that those with reconnection probabilities less than 30% should be discarded. Applying this cut removes 60% of the sample. For type II, the strings have negligible thickness but they reconnect with unit probability if they intersect. This model predicts that 27% of events are reconnected compared with 40% retained with the type I model. In both cases, the events with no assigned reconnection are replaced by the corresponding events from sample (a). The fitted masses derived from these mixed samples are greater than those obtained from the standard non-reconnected samples by 25 ± 21 MeV/c^2 and 5 ± 15 MeV/c^2 for types I and II, respectively. The type II$'$ events are similar to type II, except reconnection is suppressed if there is no reduction of the string length. In this case, 24% of events are reconnected and $\triangle m_{\mathrm{W}} = +17 \pm 15$ MeV/c^2.

For the `ARIADNE` study, the same sample of WW $\rightarrow q\bar{q}q\bar{q}$ events was hadronised using a variant, AR2 [24], which allows reconnections only when the rapidity range along the length of the string is reduced and restricts them to gluon exchanges with energies less than Γ_{W}. The fraction of events reconnected is 52%. Again, events with no resulting reconnection are replaced and then the two samples of common events compared. The fitted mass obtained from the mixed sample is shifted upwards by 27 ± 25 MeV/c^2. Other less restrictive models are not considered.

For the `HERWIG` models [23], WW events are generated using `HERWIG` also for the hard process. Three samples are fully simulated with the level of reconnection probability set to 0%, 11% (corresponding to the natural probability with three colours) and 60% respectively. The events are not identical at the primary parton level and therefore the masses derived for each case are subject to statistical fluctuations. The shifts obtained relative to the 0% connected sample are -10 and -31 MeV/c^2, respectively, with errors of $\pm$ 25 MeV/c^2 in each case.

In conclusion, none of these models, as applied, predicts any significant effect on m_{W}. The uncertainty of 25 MeV/c^2 found in the `JETSET` based models is taken as the systematic error.

The VNI model [25] has not been used to estimate a systematic error because its

current implementation does not reproduce particle momentum distributions seen in the data.

8.8 Bose-Einstein effect in the $q\bar{q}q\bar{q}$ channel

Two separate studies are made each using the primary reference sample to fit to modified Monte Carlo subsamples at the detector level. In the first, the weighting method described in [26] is implemented using a KORALW Monte Carlo sample. The Bose-Einstein strength and source radius parameters are set to values found in a recent analysis of Z peak data [27]. Comparing with the value of m_{W} obtained from the same events unweighted, a downward shift of 43 ± 25 MeV/c^2 is observed.

The second study is based on KORALW generated events with hadronisation handled by a modified PYTHIA where the Bose-Einstein correlations are described by shifts in final state like-sign boson momenta whilst ensuring that energy-momentum conservation is satisfied [28]. The strength and source radius parameters are obtained from fits to Z data. A comparison is made between mass fits in which the correlations are restricted to identical bosons within the same W and where in addition correlations between particles from different Ws are also allowed. The mass fits are made to Monte Carlo samples of the same size as the data in each case and the RMS spread of the differences in mass used to determine the error. A mean downward shift in m_{W} of 50 ± 25 MeV/c^2 is observed when Bose-Einstein effects are included between the W decay products. The larger shift is taken as the quoted systematic error.

8.9 LEP energy

The LEP beam energies are recorded every 15 minutes, or more frequently if significant shifts are observed in the RF frequency of the accelerating cavities. The instantaneous values recorded nearest in time to the selected events are used in the analysis. The relative error in the LEP energy translates into the same relative uncertainty on the fitted mass, since the beam energy is used directly in the kinematic fits. Thus, for a LEP beam energy error of $\Delta E_b = 25$ MeV [29], a systematic uncertainty of $\Delta m_{\mathrm{W}} = 21$ MeV/c^2 is assigned to all the channels. This is quoted separately from the other experimental systematic errors.

9 The results

9.1 $q\bar{q}q\bar{q}$ channel

The mass found from a maximum likelihood fit to the data is

$$m_{\mathrm{W}}^{hadronic} = 80.461 \pm 0.177(\mathrm{stat.}) \pm 0.045(\mathrm{syst.}) \pm 0.056(\mathrm{theory})\ \mathrm{GeV}/c^2.$$

The quoted theoretical error is taken from the Bose-Einstein and Colour Reconnection systematics in quadrature. The expected statistical error is obtained from fitting individually to 200 independent Monte Carlo subsamples each with the same number of events as the data taken in turn from the primary reference sample. This gives 0.178 GeV/c^2, in excellent agreement with the quoted statistical error from the fit to the data.

Table 3: Summary of the correlated and uncorrelated systematic errors on m_{W}.

	Δm_{W} (MeV/c^2)			
Source	4q	e	μ	τ
Correlated errors				
Fragmentation	35	25	25	30
Calorimeter calibrations	22	20	20	74
Tracking	-	10	10	20
Jet corrections	10	5	5	7
Initial state radiation	10	5	5	5
Uncorrelated errors				
Reference MC Statistics	10	15	13	18
Background contamination	10	6	-	10
Colour reconnection	25	-	-	-
Bose-Einstein effects	50	-	-	-
Total	72	38	37	85

Fig. 2(a) shows the mass distribution of the rescaled masses (two entries per event) in the window 60 to 86 GeV/c^2 compared with the Monte Carlo reweighted prediction.

9.2 e, μ and τ channels

The results quoting the fit statistical and experimental systematic errors are:

$$\begin{aligned}
\mathrm{WW} \to e\nu\mathrm{q\bar{q}} \quad m_{\mathrm{W}} &= 80.428 \pm 0.269(\mathrm{stat.}) \pm 0.038(\mathrm{syst.})\ \mathrm{GeV}/c^2, \\
\mathrm{WW} \to \mu\nu\mathrm{q\bar{q}} \quad m_{\mathrm{W}} &= 80.370 \pm 0.287(\mathrm{stat.}) \pm 0.037(\mathrm{syst.})\ \mathrm{GeV}/c^2, \\
\mathrm{WW} \to \tau\nu\mathrm{q\bar{q}} \quad m_{\mathrm{W}} &= 79.758 \pm 0.540(\mathrm{stat.}) \pm 0.085(\mathrm{syst.})\ \mathrm{GeV}/c^2.
\end{aligned}$$

From 460 randomly chosen subsamples taken in turn from the 400k Monte Carlo WW primary reference sample, the expected errors are ± 0.293, ± 0.309 and ± 0.557 GeV/c^2 for the e, μ and τ channels, respectively. These are in good agreement with the errors from the data. Figures 2(b),(c),(d) show the mass distributions for the selected events in each channel and the corresponding Monte Carlo distributions reweighted to the best fitted mass in each case. The weighted average result for the semileptonic channels is

$$m_{\mathrm{W}}^{semileptonic} = 80.326 \pm 0.184(\mathrm{stat.}) \pm 0.040(\mathrm{syst.})\mathrm{GeV}/c^2.$$

10 Summary and conclusions

Fully hadronic W decays are selected using a neural network method, while the semileptonic decays are identified individually using three separate selections. The mass variables are determined in a four-constraint fit with rescaling for the 4q channel, and a two-constraint fit for the semileptonic channels. The resulting invariant mass distributions

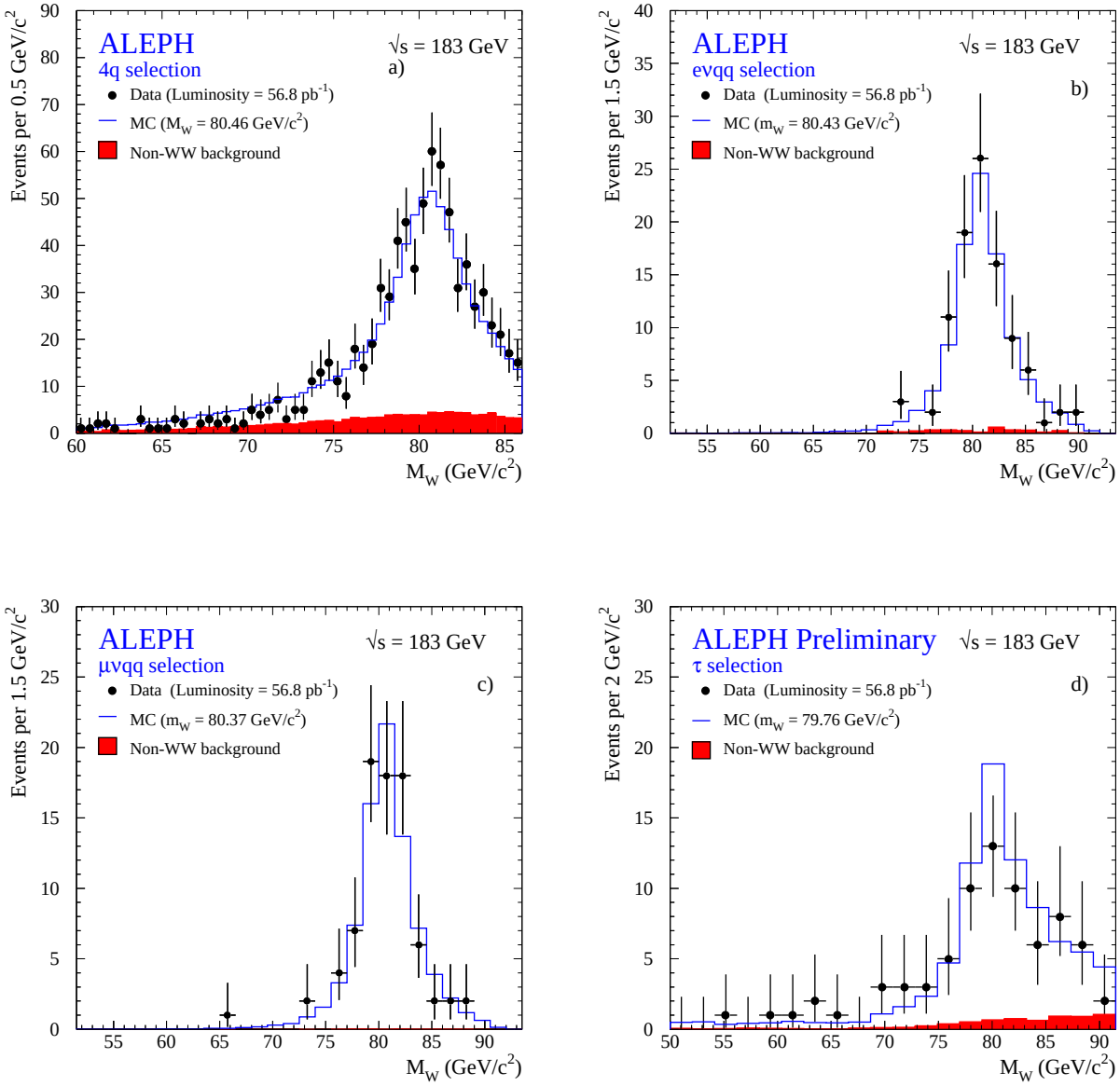

Figure 2: (a),(b),(c) and (d) Mass distributions for the 4q, e, μ, and τ data (points with error bars), non-WW background (shaded area) and signal+background Monte Carlo with m_{W} values as quoted (solid line histogram).

are compared with reweighted Monte Carlo events, and the values of the W mass are extracted in a maximum likelihood fit.

Combining all channels the average W mass from the 183 GeV data is

$$m_{\mathrm{W}} = 80.393 \pm 0.128(\mathrm{stat.}) \pm 0.041(\mathrm{syst.}) \pm 0.028(\mathrm{theory}) \pm 0.021(\mathrm{LEP}) \quad \mathrm{GeV}/c^2,$$

where the theoretical error is due to Bose-Einstein and colour reconnection uncertainties and the last error is due to the LEP energy uncertainty. The masses are combined using weights derived from the statistical and uncorrelated systematic errors added in quadrature.

The masses obtained for the hadronic and semileptonic channels separately can be combined with those determined at 172 GeV by the same final state mass reconstruction

method. This gives

$$\begin{aligned} m_{\mathrm{W}}^{hadronic} &= 80.573 \pm 0.166(\mathrm{stat.}) \pm 0.047(\mathrm{syst.}) \pm 0.049(\mathrm{theory})\ \mathrm{GeV}/c^2, \\ m_{\mathrm{W}}^{leptonic} &= 80.334 \pm 0.170(\mathrm{stat.}) \pm 0.047(\mathrm{syst.})\ \mathrm{GeV}/c^2, \end{aligned}$$

the weighted average of which is

$$m_{\mathrm{W}} = 80.451 \pm 0.119(\mathrm{stat.}) \pm 0.045(\mathrm{syst.}) \pm 0.024(\mathrm{theory}) \pm 0.022(\mathrm{LEP})\ \mathrm{GeV}/c^2.$$

Finally, the masses determined from the direct reconstruction method at 172 and 183 GeV can be combined with the earlier ALEPH results evaluated from the total W pair cross sections at 161 and 172 GeV. With a $\chi^2/ndf = 0.6/1$, this weighted average of all ALEPH current measurements of the W mass gives

$$m_{\mathrm{W}} = 80.423 \pm 0.112(\mathrm{stat.}) \pm 0.044(\mathrm{syst.}) \pm 0.021(\mathrm{theory}) \pm 0.023(\mathrm{LEP})\ \mathrm{GeV}/c^2.$$

Acknowledgments

It is a pleasure to congratulate our colleagues from the CERN accelerator divisions for the very successful operation of LEP2 despite the delayed start due to the fire in the SPS. We would also like to thank S. Jadach and K. Zalewski for their help in using `KORALW` to determine the ISR systematic error. We are indebted to the engineers and technicians in all our institutions for their contributions to the excellent performance of ALEPH. Those of us from non-member countries thank CERN for its hospitality.

References

[1] ALEPH Collaboration, *Measurement of the W mass in* $\mathrm{e^+e^-}$ *collisions at production threshold*, Phys.Lett. B401 (1997) 347.

[2] DELPHI Collaboration, *Measurement and interpretation of the W-pair cross section in* $\mathrm{e^+e^-}$ *interactions at 161 GeV*, Phys.Lett. B397 (1997) 158;
L3 Collaboration, *Pair-Production of W Bosons in* $\mathrm{e^+e^-}$ *interactions at* $\sqrt{s} = 161$ *GeV*, Phys.Lett. B398 (1997) 223;
OPAL Collaboration, *Measurement of the mass of the W boson in* $\mathrm{e^+e^-}$ *collisions at* $\sqrt{s} = 161$ *GeV*, Phys.Lett. B389 (1996) 416.

[3] ALEPH Collaboration, *Measurement of the W mass by Direct Reconstruction in* $\mathrm{e^+e^-}$ *collisions at 172* GeV, Phys.Lett. B422 (1998) 384.

[4] DELPHI Collaboration, *Measurement of the W-pair cross-section and of the W mass in* $\mathrm{e^+e^-}$ *interactions at 172 GeV*, Eur.Phys.J. C2 (1998) 581;
L3 Collaboration, *Measurements of the Mass, Width, and Gauge Couplings of the W Boson at LEP*, Phys.Lett. B413 (1997) 176;
OPAL Collaboration, *Measurements of the W boson mass and* WW *production and decay properties in* $\mathrm{e^+e^-}$ *collisions at 172 GeV*, Eur.Phys.J. C1 (1998) 395.

[5] CDF Collaboration, *A measurement of the W boson mass*, Phys.Rev. D52 (1995) 4784; DØ Collaboration, *Measurement of the W boson mass at the Fermilab* $\mathrm{p\bar{p}}$ *collider*, Phys.Rev.Lett. 80 (1998) 3008.

[6] ALEPH Collaboration, *ALEPH: A detector for electron-positron annihilations at LEP*, Nucl. Inst. Meth. A 294 (1990) 121.

[7] ALEPH Collaboration, *Performance of the ALEPH detector at LEP*, Nucl. Inst. Meth. A 360 (1995) 481.

[8] M. Skrzypek, S. Jadach, W. Placzek and Z. Wąs, Comp.Phys.Commun. 94 (1996) 216.

[9] GRACE Manual, MINAMI-TATEYA group, KEK report 92-19 (1993).

[10] T. Sjöstrand, Comp.Phys.Commun. 82 (1994) 74.

[11] W. Beenakker et al., *WW cross-section and distributions*, eds. G. Altarelli, T. Sjöstrand and F. Zwirner, CERN 96-01, vol. 1, 79.

[12] ALEPH Collaboration, *An experimental study of* $\gamma\gamma \to$ *hadrons at LEP*, Phys.Lett. B313 (1993) 509.

[13] S. Jadach, B.F.L. Ward, and Z. Wąs, Comp.Phys.Commun. 79 (1994) 503.

[14] H. Anlauf et al., Comp.Phys.Commun. 79 (1994) 466.

[15] ALEPH Collaboration, *Measurement of W-pair cross section in* $\mathrm{e^+e^-}$ *collisions at 183 GeV*, to be published.

[16] ALEPH Collaboration, *Measurement of W-pair cross section in* $\mathrm{e^+e^-}$ *collisions at 172 GeV*, Phys.Lett. B415 (1997) 435.

[17] *Determination of the mass of the* W *boson*, eds. Z. Kunszt and W.J. Stirling, CERN 96-01, vol. 1, 185.

[18] F.A. Berends, R. Pittau and R. Kleiss, Comp.Phys.Commun. 85 (1995) 437.

[19] G. Marchesini et al., Comp.Phys.Commun. 67 (1992) 465.

[20] ALEPH Collaboration, *Studies of Quantum Chromodynamics with the ALEPH Detector*, Phys.Reports 294 (1998) 1.

[21] L. Lönnblad, Comp.Phys.Commun. 71 (1992) 15.

[22] T. Sjöstrand and V.A. Khoze, Z.Phys.C 62 (1994) 281.
L. Lönnblad and T. Sjöstrand, Phys.Lett. B351 (1995) 293;
V.A. Khoze and T. Sjöstrand, CERN-TH/98-74.

[23] B. Webber in *QCD event generators*, eds. I. Knowles and T. Sjöstrand, CERN 96-01, vol. 2, 161.

[24] L. Lönnblad, Z.Phys.C70 (1996) 107.

[25] J. Ellis and K. Geiger, Phys.Lett. B504 (1997) 230.

[26] S. Jadach and K. Zalewski, CERN-TH/97-29 (1997).

[27] ALEPH Collaboration, *Bose-Einstein correlations in W-pair decays*, Contribution to ICHEP98, Paper 894; http://alephwww.cern.ch/.

[28] L. Lönnblad and T. Sjöstrand, Eur.Phys.J. C2 (1998) 165.

[29] LEP energy working group, *Evaluation of the LEP Centre-of-Mass energy above the* WW *production threshold*, CERN-EP/98-191 submitted to Eur.Phys.J.C.